Low-Frequency Spectroscopic Analysis of Monomeric and Fibrillar Lysozyme

HIDAYATUL A. ZAKARIA, BERND M. FISCHER, ANDREW P. BRADLEY, INKE JONES, DEREK ABBOTT, ANTON P. J. MIDDELBERG, and ROBERT J. FALCONER*

Australian Institute for Bioengineering and Nanotechnology, The University of Queensland, Brisbane QLD 4072, Australia (H.A.Z., A.P.J.M., R.J.F.); French-German Research Institute of Saint-Louis (ISL), 5 rue du General de Cassagnou, 68301 Saint-Louis Cedex, France (B.M.F.); School of Information Technology and Electrical Engineering, The University of Queensland, Brisbane QLD 4072, Australia (A.P.B.); and Department of Electrical and Electronic Engineering, The University of Adelaide, South Australia, SA 5005, Australia (I.J., D.A.)

Terahertz time-domain spectroscopy (THz-TDS) and Fourier transform infrared (FT-IR) spectroscopy were used to generate far-infrared and low-frequency spectral measurements of monomeric lysozyme and lysozyme fibrils. The formation of lysozyme fibrils was verified by the Thioflavin T assay and transmission electron microscopy (TEM). It was evident in the FT-IR spectra that between 150 and 350 cm^{-1} the two spectra diverge, with the lysozyme fibrils showing higher absorbance intensity than the monomeric form. The broad absorption phenomenon is likely due to light scattered from the fibrillar architecture of lysozyme fibrils as supported by simulation of Rayleigh light scattering. The lack of discrete phonon-like peaks suggest that far-infrared spectroscopy cannot detect vibrational modes between the highly ordered hydrogen-bonded beta-pleated sheets of the lysozyme subunit.

Index Headings: **Terahertz; Time-domain spectroscopy; THz-TDS; Fourier transform infrared spectroscopy; FT-IR spectroscopy; Vibrational spectroscopy; Lysozyme; Amyloid; Fibril.**

INTRODUCTION

Despite extensive research in the area, understanding of the optical properties of proteins in the far-infrared (FIR) portion of the electromagnetic spectrum between 3 and 350 cm^{-1} (0.1–12 THz) is incomplete.[1] Study of the FIR spectra of proteins was initially conducted using Fourier transform infrared (FT-IR) spectroscopy with samples prepared as water-cast protein films or protein powder mixed with polyethylene pressed into pellets.[2] A broad increase in absorbance between 100 and 200 cm^{-1} was discovered for a range of globular proteins (including lysozyme, myoglobin, and bovine serum albumin). More recent work, conducted using Fourier transform infrared (FT-IR) analysis of the proteins lysozyme, myoglobin, and bovine serum albumin all prepared as air-dried thin films, distinguished the broad band between 100 and 200 cm^{-1} and showed smaller peaks centered on 320 cm^{-1}, 380 cm^{-1}, and 410 cm^{-1}.[3] Raman spectra of peptides had bands at around 150 and 220 cm^{-1} that were assigned to disulfide linkages between the peptides.[4] Studies using terahertz time-domain (THz-TDS) analysis[5–7] and FT-IR spectroscopy with a synchrotron light source[8] have focused on the frequencies below 100 cm^{-1}. No discrete peaks are observed below 100 cm^{-1} in these studies.

The common theme of this research is that the major contribution to absorption of FIR radiation is the hydration levels in the protein.[6,7] The hydration level was used to indirectly detect conformational change in films of the protein bacteriorhodopsin.[9] The other key observation from this research was the similarity in the absorption spectra between 10 and 50 cm^{-1} (0.3–1.6 THz) of different proteins such as lysozyme and myoglobin.[4] Structured water around proteins may also be detected.[10] The differences in absorbance at 65–80 cm^{-1} (2.2–2.6 THz) between proteins in solution and the reference solution detected using a *p*-Ge laser and liquid helium detector system have been attributed to the hydration shell around the protein.[11] A recent study on β-lactoglobulin gels and polyomavirus virus-like particles illustrated potential for detecting higher-order protein structures in the spectral region of 50–450 cm^{-1}.[12] The vibrational modes causing the observed spectra for dry proteins between the frequencies 3 and 360 cm^{-1} are open for conjecture.

Studies of simpler molecules related to proteins, including N-methyl acetamide[13] and the polyamides,[14–19] have assigned bands below 360 cm^{-1} to specific mainly torsional vibrations and to intermolecular hydrogen bonding. As polyamides are prone to forming crystalline solids, many spectra are dominated by phonon-like resonances within the crystalline lattice. While proteins are less prone to formation of crystalline structures than polyamides, several peaks were observed in the FIR spectrum of crystalline lysozyme that probably correspond to phonon-like resonances within the crystalline lattice.[20] This indicates that FIR analysis of protein samples may detect phonon-like resonances if ordered structures are present.

We utilized two complementary technologies available for studying the far-infrared spectra of biological molecules: FT-IR using a liquid helium cooled bolometer with synchrotron light source and THz-TDS. Far-infrared spectroscopy has evolved over the last century[21] and has extended its capability to work at lower frequencies through the invention of the liquid-helium-cooled bolometer, Mylar beam splitters, and improved light sources such as synchrotron infrared beam lines[22] extending the frequency range down to around 20 cm^{-1}. The invention of THz-TDS is more recent[23] and has provided the ability to study frequencies ranging from 3 to 166 cm^{-1}, well below the range of conventional FT-IR spectroscopy.[24]

In this paper we studied the THz/FIR spectra of native lysozyme and lysozyme fibrils created by heat treatment at an acidic pH.[25] Native lysozyme is monomeric and has structure that includes alpha helices. Fibrils are formed by partially unfolded lysozyme molecules, which bind together with multiple hydrogen bonds to form intermolecular β-pleated sheets. Chains of these linked protein subunits form linear structures or protofilaments.[26] These protofilaments then twist around each other to form multi-chain fibrils. Fibrils are highly ordered protein structures and are obvious candidates for

Received 15 October 2010; accepted 14 December 2010.

* Author to whom correspondence should be sent. E-mail: r.falconer@uq.edu.au.

DOI: 10.1366/10-06162

0003-7028/11/6503-0260$2.00/0

analysis using FIR spectroscopy as they potentially contain multiple intermolecular hydrogen bonds capable of low-frequency vibrational modes. There are potential resonances between the repeated inter-molecular associations between lysozyme subunits, along protofilaments, along multi-filament fibrils, or between protofilaments within the fibril. The goal was to identify any phonon-like resonances within lysozyme fibrils using THz-TDS and FT-IR techniques.

MATERIALS AND METHODS

Lysozyme Monomer and Fibril Sample Preparation. Hen egg white lysozyme (Sigma Aldrich, Sydney, Australia) was dissolved in 200 ppm NaN_3 in MQ water pH 2, to a concentration of 20 mg/mL, and then dialyzed extensively with 200 ppm NaN_3 in MQ water pH 2 to remove traces of salt. Samples were then filtered through a 0.22 μm syringe filter (Millipore, North Ryde, Australia) and incubated at 57 °C for 69 h. Equal volumes of lysozyme solutions were stored at 4 °C as a negative control. The heat-treated and untreated lysozyme samples were lyophilized for 2 days. The Thioflavin T protocol described by Khurana and co-workers[27] was used to detect intermolecular beta-pleated sheets associated with fibril formation. The Thioflavin T fluorescence was measured with a Cary Eclipse fluorescence spectrophotometer (Varian Australia, Mulgrave, Australia).

Transmission Electron Microscopy. Samples were diluted to 0.2 mg/mL and 2 μL from each of the protein samples was transferred to glow-discharged, 200-mesh carbon-coated grids (Proscitech, Kirwan, Australia). Any remaining liquid on the grids was blotted with filter paper after 2 minutes. Grids were stained with 2% (w/v) uranyl acetate for 30 seconds, air-dried, and imaged with a Philips Technai 12 Microscope at 100 kV. A side-mounted Megaview II camera (Soft Imaging System GmbH, Münster, Germany) with AnalySIS software (version 3.2, Soft Imaging System GmbH) at 220 000 times magnification on the camera level was used to digitally record electron micrographs. All of these steps were performed at room temperature. Image analysis of electron micrographs was performed by visual inspection and further analysis was conducted using ImageJ software (National Institutes of Health, Bethesda, MD).

Terahertz Spectroscopy. THz spectroscopy measurements were conducted at the National T-Ray Facility, University of Adelaide, by using a commercial THz-TDS system (T-ray 2000, Picometrix, Ann Arbor, MI) driven by a Mai Tai titanium sapphire laser source (Spectra-Physics, Irvine, CA). Measurements were performed in transmission geometry, with the sample placed in the focus between the detector and emitter heads of the T-ray 2000 system. The THz beam path was shielded with a Perspex box purged with nitrogen gas to minimize water rotational lines in the THz spectra. The sample was placed in a Janis CCS-450 cryostat chamber (Wilmington, MA), where the temperature was lowered to below freezing point (20 K). A vacuum die was used to press a mixture of 20 mg protein and 180 mg polyethylene (PE) powder (Inducos, Volketswil, Switzerland) pressed at 7 tonnes for three minutes.

Far-Infrared Spectroscopy Using a Synchrotron Light Source. Spectroscopic measurements were conducted at the Australian Synchrotron, Clayton, utilizing the FIR and high-resolution beam line. The sample was mounted in a Janis ST-100FTIR cryostat (Wilmington, MA) and cooled with liquid nitrogen to 78 K. Transmission spectra were recorded using the

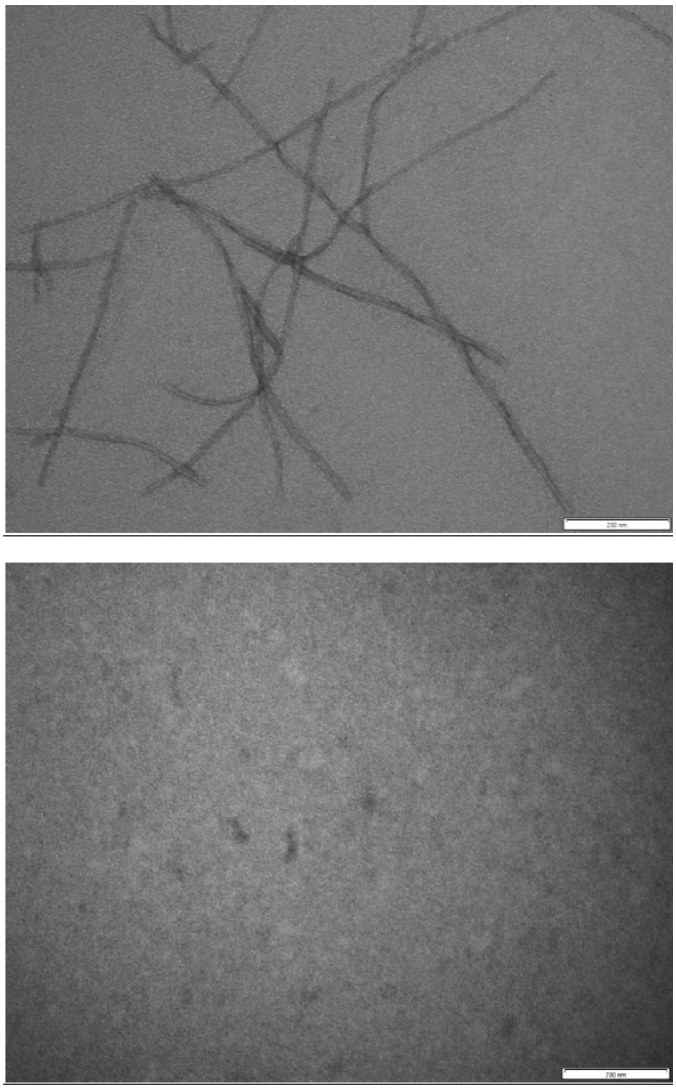

FIG. 1. TEM images of (**top**) lysozyme fibrils, indicating that the average radius for lysozyme fibrils is 4.7 nm, and (**bottom**) lysozyme monomer. Analysis of TEM images was first done by visual inspection, followed by analysis of fibrils using ImageJ software. The size bar of the figure is 200 nm.

CLS Bruker IFS 125HR Fourier transform infrared spectrometer (Bruker Optics, Ettlingen, Germany) fitted with a Mylar multilayer beam splitter, with scanner velocity of 10 kHz and a liquid-helium-cooled Si bolometer detector with aperture setting of 4 mm. The spectrum is an average of 25 interferometer scans recorded with the maximum frequency limit of 500 cm^{-1} and the resolution is 1 cm^{-1}. All spectra were filtered using a triangular finite impulse response (FIR) filter (zero phase, order 25) to reduce the etalon effect.[28] Pressed pellet samples were prepared by mixing protein samples with photometric grade polyethylene (Merck Uvasol, Germany). A vacuum die was used to press a mixture of 5 mg protein and 50 mg PE powder at a pressure of 7 tonnes for three minutes. Pure PE disks were similarly pressed as a reference.

RESULTS AND DISCUSSION

Lysozyme fibrils were formed by heat treatment at 57 °C, pH 2.0, for 69 hours. The TEM images confirmed lysozyme fibril formation (Fig. 1) and are in agreement with the study of the

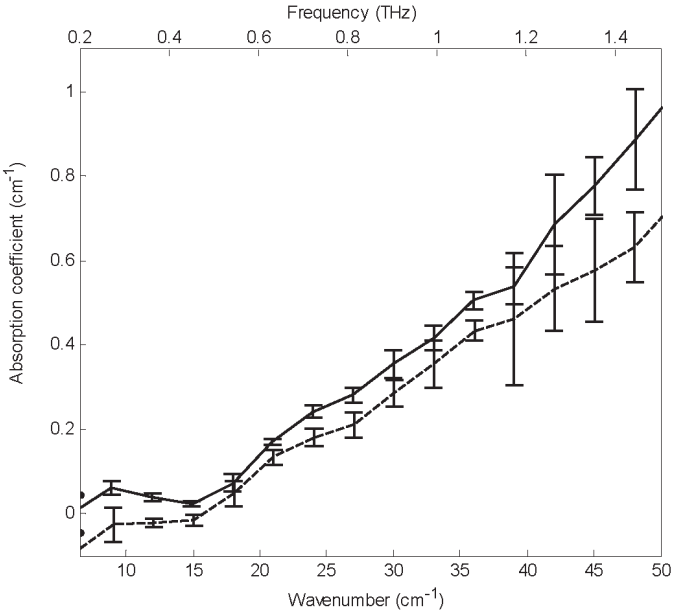

FIG. 2. THz absorption spectra of lysozyme fibrils (– – –) and monomeric lysozyme (——); error bars represent one standard deviation.

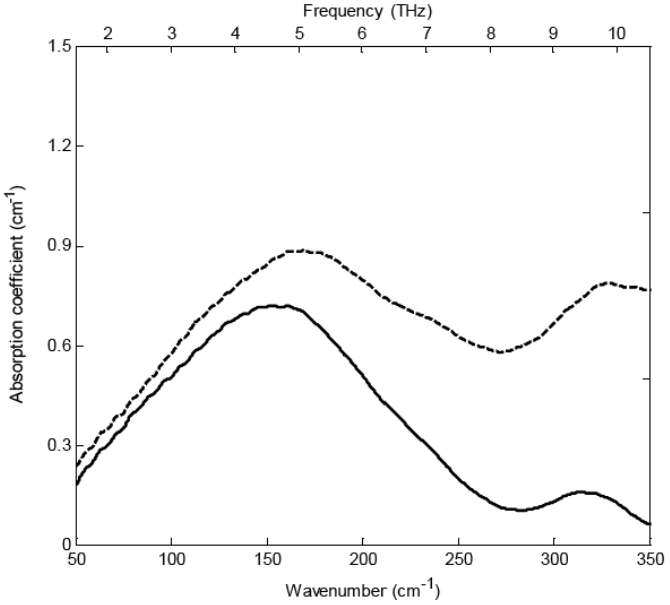

FIG. 3. FT-IR synchrotron light source absorption spectra of lysozyme fibril (– – –) and monomeric lysozyme (——). Note that the spectra diverge after 150 cm^{-1} and onwards. Standard deviation was below 0.01 A.U.

thermally induced fibrillar aggregation of lysozyme by Arnaudov et al.[25] Thioflavin T assay performed on monomer and fibrillar lysozyme confirmed the formation of fibrils in heat-treated lysozyme as the lysozyme fibrils had a higher fluorescence intensity compared to monomeric lysozyme, due to higher binding of Thioflavin T to intermolecular beta-pleated sheets present in fibrils (data not shown).

Terahertz Spectroscopy. Monomeric lysozyme and lysozyme fibrils were measured using the THz-TDS system to generate spectra between 5 and 50 cm^{-1} (0.2–1.5 THz) (Fig. 2). The absorbance of both the monomeric lysozyme and lysozyme fibrils was very low below 15 cm^{-1} and then increased monotonically with increasing frequency between the frequencies of 15 and 50 cm^{-1}. The relationship between absorbance and frequency is very similar to that observed by Knab and co-workers between 10 and 60 cm^{-1}, where no distinctive spectral features were observed in the spectra of lysozyme.[6] The featureless lysozyme absorption spectra roughly illustrates the distribution of normal modes of lysozyme as a function of frequency, where the absorption coefficients and index of refraction linearly increase with increasing water content in the lysozyme sample.[6]

The spectrum for lysozyme fibrils between 5 and 50 cm^{-1} is very similar to monomeric lysozyme and is within the observed sample-to-sample variation. There is a slight divergence in the spectra between 40 and 50 cm^{-1}. The lack of significant spectral change is consistent with the observed spectra for β-lactoglobulin fibrillar gels, which also did not differ from the monomer.[29] The spectra of monomeric and insulin fibrils between 10 and 90 cm^{-1} generated using THz-TDS showed an increase in apparent absorbance with fibril formation. However, some caution should be taken because the dynamic light-scattering data indicate that the insulin fibrils form tangled clumps potentially capable of scattering light,[30] as was seen for globular β-lactoglobulin gels.[29]

Fourier Transform Infrared Spectroscopy with a Synchrotron Light Source. FT-IR spectroscopy with a synchrotron light source, a Mylar multilayer beam splitter, and a liquid-helium-cooled Si bolometer detector was used to generate spectral measurements of monomeric lysozyme and lysozyme fibrils. It was evident that between 150 and 350 cm^{-1} the two spectra diverge, with the spectra of lysozyme fibrils showing higher absorbance than the spectra of the monomeric form (Fig. 3). Our hypothesis is that the broad absorption phenomenon is due to the light scattered from the cylindrically shaped lysozyme fibrils, further confirmed via some scattering analysis.

Rayleigh scattering is responsible for light scattering in media containing small particles with size $<< \lambda$ (wavelength). In our study the wavelength investigated at the Australian Synchrotron far-infrared beam line is from 500 μm to 19 μm and the average diameter of the lysozyme fibrils is 9.1 nm. Clearly, this diameter is much smaller than the wavelength, making Rayleigh scattering a probable phenomenon apparent in our results. The two most important parameters used in modeling the scattering efficiencies of the lysozyme fibrils are their radius and refractive index. We have presented here two methods used to calculate the Rayleigh scattering efficiencies of the fibrils, each with different values of refractive index (refractive index as a dependant or constant parameter). Figure 4 shows that the comparison between the scattering analyses with different values of refractive index made little difference. The light-scattering formula[31,32] was utilized to calculate the Rayleigh scattering efficiencies as follows.

The scattering efficiency, $Q_{sca}(\omega)$, is the result of the normalization of the scattering cross-section with the geometric cross-section.[29] The Rayleigh scattering efficiency for infinite cylinders is given by

$$Q_{sca}(\omega) = \frac{2}{x(\omega)}\left[|b_0(\omega)|^2 + 2|b_1(\omega)|^2\right] \quad (1)$$

where $b_0(\omega) \approx \{-i\pi x(\omega)^2[m(\omega)^2 - 1]\}/4$ and $b_1.(\omega) \approx \{-i\pi x(\omega)^4[m(\omega)^2 - 1]\}/32$ Here $m(\omega)$ and $x(\omega)$ are the

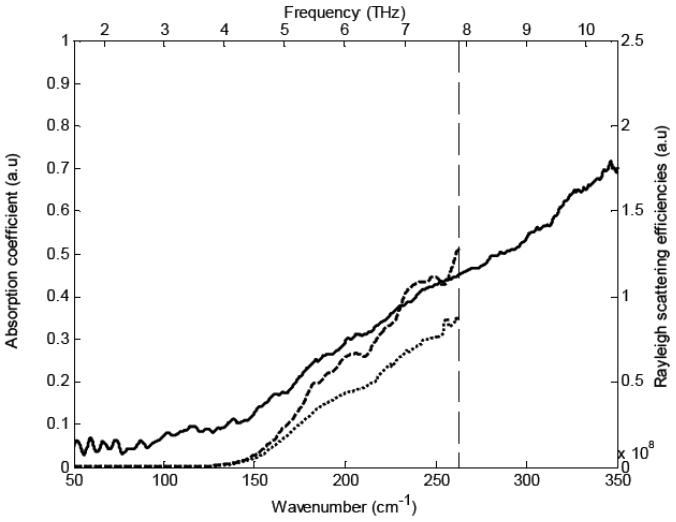

FIG. 4. The difference spectrum of lysozyme fibrils and monomeric lysozyme (——), and the Rayleigh scattering efficiencies with calculated (- - -) and constant (– – –) refractive index. Note that over 250 cm^{-1} the signal-to-noise ratio was too great to calculate the Rayleigh scattering efficiency.

refractive index ratio of the sample and air (Eq. 2) and the size parameter of the sample (Eq. 4), respectively.

The refractive index ratio of the sample ($n_s(\omega)$) and the surrounding medium ($n_{sm}(\omega)$) was calculated using

$$m(\omega) = \frac{n_s(\omega)}{n_{sm}(\omega)} \tag{2}$$

where $n_{sm}(\omega) \approx n_{air}(\omega) \approx 1$ and the complex refractive index of the sample $\hat{n}_s(\omega)$ is given by

$$\hat{n}_s(\omega) = n(\omega) + \frac{i\alpha_s(\omega)c}{2\omega} \tag{3}$$

where $n(\omega)$ is the index of refraction of the sample, $\alpha_s(\omega)$ is the absorption of the sample, and c is the speed of light.

The size parameter of the fibrils was calculated using

$$x(\omega) = \frac{2\pi n_s(\omega) r}{\lambda} \tag{4}$$

where r is the radius of the fibrils and λ is the wavelength.

The refractive index used in this model was obtained from the interferogram data of the sample's FT-IR measurements. The useful range of the FT-IR measurement is from 20 to 500 cm^{-1}. Shown here is the calculation used to obtain the refractive index.[32]

It is essential to remember that there is a one-to-one relationship between an interferogram and its spectrum. The mathematical relationship between the two is the Fourier transform, where the interferogram is the Fourier transform of the spectrum of the light. Hence, to obtain the spectrum of the light source producing the interferogram, an inverse Fourier transform must be applied to the interferogram. The complex inverse Fourier transform of the sample interferogram was computed with a real part $P(\omega)$ and imaginary part $Q(\omega)$. The same computation was also performed on the reference interferogram, where the real part is $P_r(\omega)$ and the imaginary part is $Q_r(\omega)$. The complex inverse Fourier transform of the interferogram yields the spectra equation, which is explained in detail by Bell.[33]

The modulus of the reflection coefficient is given by

$$R(\omega) = \sqrt{\frac{P^2(\omega) + Q^2(\omega)}{P_r^2(\omega) + Q_r^2(\omega)}} \tag{5}$$

The reflection phase angle of the sample is given by

$$\varphi(\omega) = \pi + \arctan\left[\frac{Q(\omega)}{P(\omega)}\right] \tag{6}$$

The real part of the index of refraction $n(\omega)$ is then given by

$$n(\omega) = \frac{[1 - R^2(\omega)]}{[1 + 2R(\omega)\cos\varphi(\omega) + R^2(\omega)]} \tag{7}$$

A comparison of the Rayleigh scattering efficiency of lysozyme fibrils using two different values of refractive index showed little deviation between them, as already demonstrated in Fig. 4, except that when utilizing a constant refractive index value, the magnitude of the scattering efficiencies is slightly higher compared to the scattering efficiencies calculated from the measurement-dependant refractive index. This observation might be attributed to the fact that the refractive index intensity at higher wavenumbers (50–300 cm^{-1}) might be higher than that from the refractive index readings obtained from THz measurements (20–150 cm^{-1}). Previous studies have shown that light scattering contributes toward spectral variance in human epithelial cells,[34] β-lactoglobulin gels,[29] and monodispersed poly(methyl methacrylate) (PMMA) spheres.[35]

The estimated refractive index is commonly used to model scattering efficiencies in other studies.[33,34] In our case, we have used a refractive index of 1.5, measured from THz spectroscopy readings of the same lysozyme fibril samples where the useful range of the THz measurement is from 20 to 150 cm^{-1}. Shown here in Fig. 4 is the Rayleigh scattering of lysozyme fibrils using a constant refractive index as one of its parameters. Starting from 150 cm^{-1}, a linear rise in Rayleigh scattering efficiency was observed, indicating that from 150 cm^{-1} the cylindrical structure of lysozyme fibrils scatters light.

Fourier transform infrared spectroscopy of monomeric lysozyme and lysozyme fibrils was carried out on three separate occasions. Fresh fibrils were prepared for each experiment. The shape of the spectra was consistent. Variability from sample to sample within an experiment was very low. There was some variation between batches in the magnitude of the divergence in absorbance between the lysozyme fibrils and monomeric lysozyme after 150 cm^{-1}; this was also observed in the magnitude of the Thioflavin T fluorescence, indicating that it was due to the extent of fibril formation rather than to the far-infrared spectroscopic analysis. The quality of the polyethylene used in making the pressed pellets was critical for generating acceptable spectra across the 50–350 cm^{-1} range. In our experience photometric grade polyethylene (Merck Uvasol, Germany) produced the best results.

CONCLUSION

In this paper we have demonstrated that THz spectroscopy was poor at differentiation of fibrillar and monomeric lysozyme structures. Far-infrared spectroscopy with a synchrotron light source, Mylar beam splitter, and a liquid-helium-cooled

bolometer was able to differentiate between fibrillar and non-fibrillar structures. This is most likely due to Rayleigh scattering caused by the ability of the cylindrically shaped fibrils to scatter light with a frequency greater than 150 cm^{-1}. From this work we can conclude that higher frequency (greater than 150 cm^{-1}) is necessary to detect formation of fibrils in proteins.

All the observed differences in the spectra of monomeric and lysozyme fibrils observed between 50 and 350 cm^{-1} can be explained by light scattering. The lack of changes to the spectrum, due to vibrational changes, occurs despite the secondary and higher-order structural change of the protein associated with fibril formation. Secondary structural changes during fibril formation are pronounced; alpha-helical structures are lost and replaced with intermolecular beta-pleated sheets. This resulted in a marked difference in the amide backbone and can be seen as a shift in the amide I peak (1600–1700 cm^{-1}).[36] The fibrils seen by TEM are held together by countless hydrogen bonds that hold the beta-pleated sheet structure together. Hydrogen bonds in crystalline lattices generate obvious phonon-like bands in the THz-FIR part of the spectrum, so the lack of similar bands in lysozyme fibrils is disappointing. The observed lack of features (other than those assigned to light scattering) is consistent with β-lactoglobulin fibrillar gels and arguably with insulin fibrils.[30]

A previous study was able to identify significant changes to the THz/FIR spectrum of polyomavirus virus-like particles on self-assembly that could not be attributed to light scattering (these are icosahedral structures of viral capsid protein with a radius of approximately 25 nm).[12] Evidently FT-IR spectroscopy with a synchrotron or equivalent light source, a Mylar multilayer beam splitter, and a liquid-helium-cooled Si bolometer detector can be used to detect structural changes in protein assemblies using the bandwidth between 50 and 350 cm^{-1}. While some structures such as polyomavirus virus-like particles are amenable to this approach, the only impact of lysozyme fibrils is on light scattering and not on absorbance, limiting its usefulness in studying this phenomenon.

ACKNOWLEDGMENTS

This work was funded by the Australian Research Council grant number DP0773111 and supported by the National Collaborative Research Infrastructure Strategy, an Australian Federal Government initiative. We thank the Australian Synchrotron for access to their infrared beamline, Dominique Appadoo of the Australian Synchrotron for his assistance, and Yuan Yuan Fan and Cherrine Chan of the Australian Institute for Bioengineering and Nanotechnology for the electron microscopy.

1. W. Withayachumnankul, G. G. Png, X. X. Yin, S. Atakaramians, I. Jones, H. Lin, B. S. Y. Ung, J. Balakrishnan, B. W.-H. Ng, B. Ferguson, S. P. Mickan, B. M. Fischer, and D. Abbott, Proc. IEEE **95,** 1528 (2007).
2. U. Buontempo, C. Careri, P. Fasella, and A. Ferraro, Biopolymers **10,** 2377 (1971).
3. S. C. Shen, L. Santo, and L. Genzel, Int. J. Infrared Milli. Wave **28,** 595 (2007).
4. N. N. Brandt, A. Y. Chikishev, A. V. Kargovsky, M. M. Nazarov, O. D. Parashchuk, D. A. Sapozhnikov, I. N. Smirnova, A. P. Shkurinov, and N. V. Sumbatyan, Vib. Spectrosc. **47,** 53 (2008).
5. A. Markelz, S. Whitemire, J. Hillebrecht, and R. Birge, Phys. Med. Biol. **47,** 3797 (2002).
6. J. Knab, J. Y. Chen, and A. Markeltz, Biophys. J. **90,** 2576 (2006).
7. C. F. Zhang and S. M. Durbin, J. Phys. Chem. B **110,** 23607 (2006).
8. K. D. Moeller, G. P. Williams, S. Steinhauser, C. Hirschmugl, and J. C. Smith, Biophys. J. **61,** 276 (1992).
9. S. E. Whitemire, D. Wolpert, A. G. Markelz, J. R. Hillebrecht, J. Galan, and R. R. Birge, Biophys. J. **85,** 1269 (2003).
10. T. M. Greve, K. B. Andersen, A. Engdahl, B. Nelander, and O. F. Nielsen, AIP Conf. Proc. **1075,** 13 (2008).
11. S. Ebbinghaus, S. J. Kim, M. Heyden, X. Yu, M. Gruebele, D. M. Leitner, and M. J. Havenith, Am. Chem. Soc. **130,** 2374 (2008).
12. R. J. Falconer, H. Zakaria, Y. Y. Fan, A. P. Bradley, and A. P. J. Middelberg, Appl. Spectrosc. **64,** 1259 (2010).
13. K. Itoh and T. Shimanouchi, Biopolymers **5,** 921 (1965).
14. Y. Abe and S. Krimm, Biopolymers **11,** 1817 (1972).
15. Y. Abe and S. Krimm, Biopolymers **11,** 1841 (1972).
16. W. H. Moore and S. Krimm, Biopolymers **15,** 2439 (1976).
17. W. H. Moore and S. Krimm, Biopolymers **15,** 2465 (1976).
18. K. Itoh, T. Nakahara, and T. Shimanouchi, Biopolymers **6,** 1759 (1968).
19. K. Itoh, T. Shimanouchi, and M. Oya, Biopolymers **7,** 649 (1969).
20. M. Ataka and S. Tanaka, Biophys. J. **18,** 507 (1979).
21. E. Hagen and H. Rubens, Annalen Der Physik **8,** 1 (1902).
22. G. P. Williams, Int. J. Infrared Milli. Waves **5,** 829 (1984).
23. D. H. Auston, K. P. Cheung, and P. R. Smith, Appl. Phys. Lett. **45,** 284 (1984).
24. P. U. Jepsen and B. M. Fischer, Opt. Lett. **30,** 29 (2005).
25. L. N. Arnaudov and R. de Vries, Biophys. J. **88,** 515 (2005).
26. M. R. M. Krebs, D. K. Wilkins, E. W. Chung, M. C. Pitkeathly, A. K. Chamberlain, J. Zurdo, C. V. Robinson, and C. M. Dobson, J. Mol. Biol. **300,** 541 (2000).
27. R. Khurana, C. Coleman, C. Ionescu-Zanetti, S. A. Carter, V. Krishna, R. K. Grover, R. Roy, and S. J. Singh, Struct. Biol. **151,** 229 (2005).
28. S. J. Orfanidis, *Introduction to Signal Processing* (Prentice-Hall, Englewood Cliffs, NJ, 1996), pp. 434–444.
29. G. M. Png, R. J. Falconer, B. M. Fischer, H. A. Zakaria, S. P. Mickan, A. P. J. Middelberg, and D. Abbott, Opt. Exp. **17,** 13102 (2009).
30. R. Liu, M. X. He, R. X. Su, Y. J. Yu, W. Qi, and Z. M. He, Biochem. Biophys. Res. Commun. **391,** 862 (2010).
31. C. F. Bohren and D. R. Huffman, *Absorption and Scattering of Light by Small Particles* (John Wiley and Sons, New York, New York, 1998), pp. 130–154.
32. H. C. Hulst, *Light Scattering by Small Particles* (Dover Publications, New York, 1981), pp. 63–73.
33. R. J. Bell, *Introductory Fourier Transform Spectroscopy* (Academic Press, London, 1981), pp. 81–51.
34. B. Mohlenhoff, M. Romeo, M. Diem, and B. R. Woody, Biophys. J. **88,** 3635 (2005).
35. P. Bassan, H. J. Byrne, F. Bonnier, J. Lee, P. Dumas, and P. Gardner, Analyst (Cambridge, U.K.) **134,** 1586 (2009).
36. A. Hedoux, R. Ionov, J. F. Willart, A. Lerbret, F. Affouard, Y. Guinet, M. Descamps, D. Prevost, L. Paccou, and F. Danede, J. Chem. Phys. **124,** 014703 (2006).